7636 *Biochemistry* **2009,** *48,* 7636–7645
DOI: 10.1021/bi900031w

BIOCHEMISTRY
including biophysical chemistry & molecular biology
Article

Biochemical and Structural Characterization of the Human TL1A Ectodomain[†,‡]

Chenyang Zhan,[§] Qingrong Yan,[∥] Yury Patskovsky,[§] Zhenhong Li,[§] Rafael Toro,[§] Amanda Meyer,[§] Huiyong Cheng,[§] Michael Brenowitz,[§] Stanley G. Nathenson,[∥,⊥] and Steven C. Almo*[,§]

[§]*Departments of Biochemistry and* [∥]*Cell Biology and* [⊥]*Microbiology and Immunology, Albert Einstein College of Medicine, Bronx, New York 10461*

Received January 8, 2009; Revised Manuscript Received May 10, 2009

ABSTRACT: TNF-like 1A (TL1A) is a newly described member of the TNF superfamily that is directly implicated in the pathogenesis of autoimmune diseases, including inflammatory bowel disease, atherosclerosis, and rheumatoid arthritis. We report the crystal structure of the human TL1A extracellular domain at a resolution of 2.5 Å, which reveals a jelly-roll fold typical of the TNF superfamily. This structural information, in combination with complementary mutagenesis and biochemical characterization, provides insights into the binding interface and the specificity of the interactions between TL1A and the DcR3 and DR3 receptors. These studies suggest that the mode of interaction between TL1A and DcR3 differs from other characterized TNF ligand/receptor complexes. In addition, we have generated functional TL1A mutants with altered disulfide bonding capability that exhibit enhanced solution properties, which will facilitate the production of materials for future cell-based and whole animal studies. In summary, these studies provide insights into the structure and function of TL1A and provide the basis for the rational manipulation of its interactions with cognate receptors.

TNF-like 1A (TL1A),[1] also known as vascular endothelial growth inhibitor (VEGI), is a newly described member of the TNF superfamily involved in a wide range of human pathologies, including autoimmunity and tumor progression (*1*). The functional receptor of TL1A is death receptor 3 (DR3), a TNF receptor family member that contains a cytoplasmic death domain. TL1A is expressed by endothelial and dendritic cells, and its expression in human umbilical vein endothelial cells (HUVEC) is significantly enhanced by treatments with TNF-α or IL-1 but reduced by IFN-γ (*1*). DR3 is predominantly expressed by activated T-cells and to a lesser extent by endothelial cells (*2*, *3*). Engagement of DR3 by TL1A expressed on dendritic cells triggers a costimulatory signal in T-cells that induces the secretion of IFN-γ via NF-κB-associated pathways (*1*, *4*). The treatment of DR3-expressing tumor cell lines with recombinant soluble TL1A results in caspase-dependent apoptosis when proliferative signals are blocked by the protein synthesis inhibitor cycloheximide (*1*). Similarly, overexpression of secreted TL1A protein from vascular endothelial cells results in autocrine apoptosis, which may function to inhibit tumor neovascularization and progression (*2*, *3*). Notably, mice deficient in either TL1A or DR3 exhibit normal immune system development; however, both strains show significant reductions in the development of autoimmune diseases, highlighting an important role for the TL1A−DR3 interaction in autoimmune pathology (*5*, *6*).

The TL1A−DR3 interaction can be inhibited by the DcR3 decoy receptor (*1*), a soluble TNFR family member that is expressed by a wide range of normal human tissues, particularly adult spleen, colon, and lung (*7*, *8*). In addition to TL1A, DcR3 also neutralizes the TNF family members LIGHT (*9*) and FasL (*8*). Although the gene coding for DcR3 is absent from the murine genome, transgenic mice ubiquitously expressing human DcR3 exhibit systematically attenuated Th1 responses (*10*). *In vitro* studies demonstrated that the treatment of dendritic cells with DcR3 polarizes T-cell development toward a Th2 response (*11*, *12*). In addition to the modulation of immune function, DcR3 can induce angiogenesis and neovascularization by inhibiting the autocrine effect of TL1A (*3*). Based on these results and the observation that DcR3 overexpression is associated with the development of a variety of malignancies (*7*, *8*, *13*), it has been suggested that tumor cells might secrete DcR3 as an immune evasion mechanism that inhibits T-cell function through neutralization of TNF ligands and may further promote neovascularization (*3*, *8*). Additionally, transgenic NOD mice that express DcR3 specifically in pancreatic β-islets showed localized suppression of Th1 cells and protection from autoimmune diabetes (*14*). Interpretation of these results is complicated by the multiple interactions involving DcR3, which results in a complex interrelationship between multiple signaling pathways. Detailed knowledge of these interactions, and their

[†]This work was supported by NIH Grants AI07289 (to S.G.N. and S.C.A.), the Albert Einstein Cancer Center (P30CA13330), and the Albert Einstein Macromolecular Therapeutics Development Facility.

[‡]The structures of the wild-type TL1A protein and two mutant proteins, C95S and C95S/C135S, have been deposited to the PDB as entries 2QE3, 2RJK, and 2RJL, respectively.

*To whom correspondence should be addressed. Tel: (718) 430-2746. Fax: (718) 430-8565. E-mail: almo@aecom.yu.edu.

[1]Abbreviations: TNF, tumor necrosis factor; TNFR, tumor necrosis factor receptor; TL1A, TNF-like 1A; SPR, surface plasmon resonance.

 Published on Web 06/12/2009

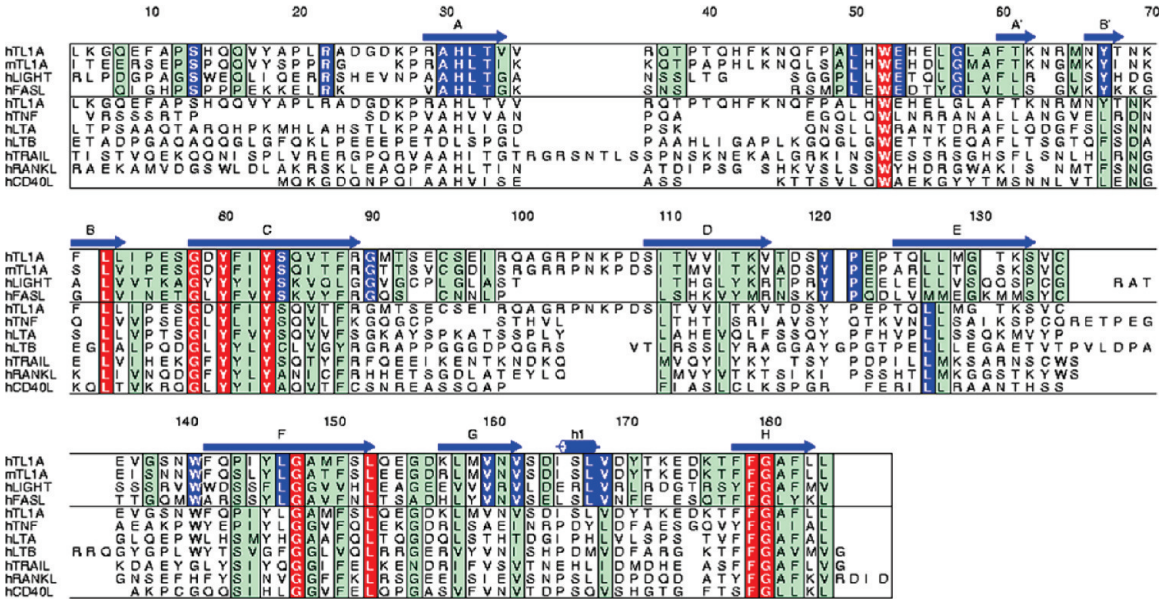

FIGURE 1: Sequence alignment of conventional TNF ligands. Those ligands capable of binding human DcR3 (TL1A, mouse TL1A, LIGHT, FasL) are treated as a group (upper four sequences). The remaining conventional ligands are displayed below the black line. Residues that are identical in only one of the two groups are shown in blue. Residues that are identical in both groups are shown in red. Additional conserved residues are colored green. Secondary structure of TL1A is displayed atop the alignment, with arrows representing β-strands and a cylinder representing the α-helix. The numbering is based on the sequence of human TL1A ectodomain and is consistently referenced in the text. With the exception of murine TL1A, all proteins are from *Homo sapiens*.

contributions to signaling, will aid in the development of therapeutic strategies for both cancer and autoimmune diseases.

Based on sequence homology, TL1A belongs to the conventional TNF ligand family, which currently includes eight other members: FasL, LIGHT, TNFα, LTα, LTβ, TRAIL, RANKL, and CD40L (Figure 1) (*15*). Members of the TNF superfamily are typically type II transmembrane proteins that form noncovalent homotrimers composed of β-sandwich "jelly-roll" protomers. DR3 and DcR3 belong to the TNFR superfamily that is composed of type I transmembrane proteins or secreted proteins characterized by pseudorepeats of between one to six extracellular cysteine-rich domains (CRDs). The three reported structures of TNF ligand/receptor complexes (LTα/TNFR1; TRAIL/DR5; OX40L/OX40) exhibit a similar overall organization, in which the trimeric ligands recruit three receptor molecules to form a 3-fold symmetric assembly with a 3:3 receptor-to-ligand stoichiometry (*16*−*18*). In these complexes, the receptor binding surfaces are located at the interfaces formed between two ligand protomers, and there are no interactions between receptor molecules.

Upon ligand binding, depending on the composition of the intracellular domain and cellular contexts, TNFRs recruit either TNF receptor associated factors (TRAF) or death domain adapter proteins. Generally, the recruitment of TRAFs induces the activation of NF-κB-mediated pathways, which initiate transcriptional programs for proinflammatory cytokine production and cellular proliferation; in contrast, the recruitment of death domain adapter proteins activates caspases and leads to apoptosis (*19*). These pathways represent major targets for therapeutic intervention. For example, Enbrel, a soluble TNF receptor (TNFR)−Ig fusion protein, and Remicade, a monoclonal antibody against TNF-α, both sequester TNF-α and block activation of TNFR-associated inflammatory responses. These reagents represent leading treatments for inflammatory diseases, including rheumatoid arthritis and inflammatory bowel disease.

TL1A-associated pathways also represent targets of potential therapeutic importance, as they are implicated in the pathogenesis of several inflammatory diseases, including inflammatory bowel disease (*4*), atherosclerosis (*20*), and rheumatoid arthritis (*21*). In particular, the involvement of TL1A in Crohn's disease has been suggested on the basis of mouse models (*4*) and the correlation of disease with single nucleotide polymorphisms in the TL1A gene (*22*). As a consequence, TL1A-associated signaling pathways are promising therapeutic targets for Crohn's disease (*4*, *23*). In this light, it will be of considerable clinical importance to develop TL1A-directed reagents, such as soluble DR3 receptor, soluble DcR3, or blocking antibodies directed against TL1A (*4*, *23*). Here, we report the crystallographic and biochemical characterization of the extracellular domains of TL1A that suggests a mode of receptor recognition distinct from other TNF family members. In addition, we describe a series of fully functional cysteine mutants with enhanced solution behavior. These studies provide insights into the function of this important cytokine and facilitate the manipulation of its interactions with DR3 and DcR3.

EXPERIMENTAL PROCEDURES

Cloning, Overexpression, Mutagenesis, and Purification of TL1A. TL1A cDNA was obtained from a human kidney cDNA library (BioChain, Hayward, CA) by PCR. The extracellular domain of human TL1A (L72-L251) was cloned into pET28a vector and expressed with an N-terminal His tag in *Escherichia coli* strain BL21-AI (Invitrogen, Carlsbad, CA). In this strain, expression of a chromosomal copy of the T7 RNA polymerase gene is under the tight control of the arabinose-inducible araBAD promoter. The cells were grown in LB medium supplemented with kanamycin (50 μg/mL) at 37 °C to an OD_{600} of 0.5, and protein expression was induced by addition of 0.2% arabinose and 1 mM IPTG. Cells were harvested by centrifugation after an additional 20 h of growth (250 rpm, 20 °C), resuspended in lysis buffer (50 mM NaH_2PO_4, pH 8, 300 mM NaCl, 20 mM imidazole, 5 μg/mL DNase I), and lysed by French press. The lysate was clarified by centrifugation at 48384*g* for

30 min and the supernantant applied to Qiagen Ni-NTA agarose resin (Qiagen, Valencia, CA). After being washed with 50 mL of wash buffer (50 mM NaH_2PO_4, pH 8.0, 300 mM NaCl, 50 mM imidazole), fractions that were eluted with elution buffer (50 mM NaH_2PO_4, pH 8.0, 300 mM NaCl, 250 mM imidazole) were pooled and dialyzed against 50 mM MES (pH 6.5), supplemented with 20 mM NaCl and 4 mM βME. The His tag was cleaved with thrombin, and the TL1A protein was purified to homogeneity by cation-exchange chromatography (FPLC) using a Mono S HR 10/10 column (Pharmacia). For crystallization, the purified protein was dialyzed into 10 mM Tris (pH 8.0), supplemented with 100 mM NaCl, 1 mM βME, and 1 mM cysteamine.

TL1A point mutations were generated with the QuikChange site-directed mutagenesis kit (Stratagene, La Jolla, CA), and the mutant proteins were purified as described for the wild type.

Crystallization, Structure Determination, and Refinement. Diffraction quality crystals of TL1A were obtained by sitting drop vapor diffusion at 17 °C by mixing 1 μL of protein (10 mg/mL) with 1 μL of reservoir solution (0.1 M Tris-HCl, pH 8.5, 20% methanol, and 0.01 M $CaCl_2$) and allowing for equilibration over 1 mL of reservoir. C95S and C95S/C135S mutant proteins were crystallized under the same conditions, but the optimal protein to reservoir solution ratio was 1:2 and 2:1 for C95S and C95S/135S mutants, respectively. Cubic-shaped crystals typically appeared after 1 week. Prior to X-ray data collection, crystals of wild-type TL1A were flash cooled in liquid nitrogen after cryoprotection with mother liquor supplemented with 30% glycerol. Mutant TL1A crystals were cryoprotected in 20% PEG 400, 50% 2-propanol, 0.1 M Tris, pH 8.5, and 0.01 M $CaCl_2$ prior to flash cooling. All TL1A crystals exhibited diffraction consistent with the cubic space group $P4_132$ (unit cell: $a = b = c = 120.4$ Å), with 1 monomer in the asymmetric unit. Data were collected at the X29 beamline of the National Synchrotron Light Source (Brookhaven National Laboratory, Upton, NY), using a ADSC Quantum-315 CCD detector and 1.0809 Å radiation. The wild-type, C95S mutant, and C95S/C135S mutant crystals diffracted to resolutions of 2.5, 2.3, and 2.05 Å, respectively.

Diffraction data were integrated and scaled with the HKL2000 software package (*24*). An initial structure of wild-type TL1A was determined by molecular replacement with the program PHASER 1.1 (*25*), using TNF-α monomer (PDB code 2TNF) as the search model. The remainder of the model was built with ARP/WARP (*26*) and refined with REFMAC5 (*27*). The mutant TL1A structures were solved by difference Fourier methods. Data collection and refinement statistics are presented in Table 1. Atomic coordinates and structure factors of the wild-type protein and two mutant proteins, C95S and C95S/C135S, have been deposited to the PDB and are available under the accession codes 2QE3, 2RJK, and 2RJL, respectively. Subsequent to the release of our wild-type TL1A structure, another human wild-type TL1A structure was reported (PDB codes 2RE9 and 2O0O) (*28*). These structures are similar with rmsds of about ~0.9 Å for 139 C_α atoms and 0.33 Å for 125 C_α atoms excluding disordered regions (Suporting Information Figure 1).

Solution Characterization. The oligomeric state of the wild-type TL1A ectodomain was examined by sedimentation velocity with a Beckman XL-I analytical ultracentrifuge. Proteins at three concentrations (10.7, 26.7, and 47.3 μM) were prepared in 10 mM Tris buffer (pH 8.0) containing 100 mM NaCl and 1 mM TCEP. The sedimentation velocity experiments were performed at 45000 rpm with a Ti-60 rotor and double-sector cells at 20 °C. The sedimentation boundaries were monitored by the absorption at 280 nm and analyzed using DCDT+ software (*29*). The partial specific volume, buffer densities, and viscosities were calculated using program SEDNTERP (*30*) and were used to correct the resulting sedimentation values to standard conditions, $s_{20,w}$.

The TL1A ectodomain and DcR3 cysteine-rich domain (CRD) were also examined by size exclusion chromatography on a Superdex 200 column. Purified TL1A and DcR3-CRD proteins (see Supporting Information for expression and purification of DcR3-CRD) were mixed in a 1:1 ratio at a final total concentration of 1 mg/mL and incubated at room temperature for 2 h. TL1A alone (5 mg/mL) and the incubated TL1A/DcR3 mix were applied to a Superdex-200 column equilibrated with 10 mM Tris (pH 8.0) and 100 mM NaCl and eluted using the same buffer at a flow rate of 0.5 mL/min. The column was calibrated with cytochrome *c* (12.4 kDa), carbonic anhydrase (29 kDa), albumin (66 kDa), and alcohol dehydrogenase (150 kDa) using the protocol described above.

SDS−Polyacrylamide Gel Electrophoresis. Samples for nonreducing SDS−PAGE were prepared by mixing freshly purified protein and Laemmli sample buffer (Bio-Rad, Hercules, CA) with no addition of reducing agents. After being boiled for 2 min, the samples were loaded onto precast 4−20% gradient gels (Bio-Rad, Hercules, CA), and electrophoresis was performed at 200 V for 38 min, using chamber buffer composed of 25 mM Tris (pH 8.0), 192 mM glycine, and 1% SDS. Gels were stained with Coomassie blue. To prepare reducing SDS−PAGE, β-mercaptoethanol was included in the sample buffer at a final concentration of 5%.

Surface Plasmon Resonance (SPR) Binding Assay. SPR binding assays were performed with a BIAcore 3000 optical biosensor at 25 °C. Recombinant human DcR3−Ig fusion protein (R&D Systems, Minneapolis, MN) was immobilized on CM5 sensor chips by free amine coupling. TL1A mutant and wild-type proteins were injected over the sensor chip at a concentration of 10 nM. The maximum association response of each mutant is divided by that of the wild-type TL1A and represented as percentage of wild-type binding response. All mutants were generated in the C95S/C135S background, as this double mutant exhibited superior solution behavior compared to the wild-type protein while maintaining the same DcR3 binding affinity (see below and Suporting Information Figure 3).

Thermal Stability of TL1A mutants. The fluorescence-monitored thermal denaturation of wild-type and mutant TL1A was performed using the iQ5 real-time PCR detection system (Bio-Rad). Briefly, 20 μL of each protein at 10 μM concentration was mixed with 0.5 μL of 200× Sypro orange solution and pipetted into separate wells of a 96-well PCR plate. After centrifugation to remove air bubbles, the plate is loaded into the PCR machine and the temperature ramped from 20 to 99 °C, in 1 °C increments with a dwell time of 6 s. The negative first derivative of the fluorescence change (−dRFU/dT) for each protein is plotted against temperature, and the melting temperature is defined as the minimum in the −dRFU/dT curve.

RESULTS

Overall Structure. The crystal structure of the human TL1A extracellular domain was determined by molecular replacement and refined to a resolution of 2.5 Å (Table 1). TL1A adopts the jelly-roll fold typical of the TNF family, with inner and outer β-sheets composed of the A′AHCF and B′BGDE strands,

Table 1: Statistics for Data Collection and Refinement

	WT	C95S	C95S/C135S
	Data Collection		
PDB code	2QE3	2RJK	2RJL
space group	$P4_132$	$P4_132$	$P4_132$
unit cell lengths (Å)	a = 120.40	a = 118.23	a = 117.58
	b = 120.40	b = 118.23	b = 117.58
	c = 120.40	c = 118.23	c = 117.58
unit cell angles (deg)	α = 90.00	α = 90.00	α = 90.00
	β = 90.00	β = 90.00	β = 90.00
	γ = 90.00	γ = 90.00	γ = 90.00
wavelength used (Å)	1.0809	1.0809	1.0809
resolution range (Å)	2.5−19.8	2.3−25.8	2.05−27.7
sweep range (deg) (exposure time, s)	180 (3)	150 (1)	130 (1)
unique reflections (N)	10462	12705	17323
redundancy[a]	21.1 (10.6)	22.0(15.9)	21.0 (8.6)
completeness (%)[a]	99.9 (100)	99.9 (100)	99.3 (93.1)
R_{merge}[a,b]	0.17 (0.566)	0.085 (0.878)	0.101 (0.830)
$\langle I/\sigma I\rangle$[a]	8.43 (1.6)	40.5 (3.33)	30.6 (2.2)
	Refinement		
resolution range (Å)	2.5−19.8	2.3−25.8	2.05−27.7
R_{work}[a,c]	0.211 (0.395)	0.212 (0.212)	0.209 (0.213)
R_{free}[a]	0.263 (0.525)	0.265 (0.326)	0.244 (0.294)
average B-factors (Å^2), protein	51.4	52.7	40.3
average B-factors (Å^2), water	46.7	52.1	41.8
rms bonds (Å)	0.027	0.019	0.011
rms angles (deg)	2.355	1.682	1.281
residues in most favored region (%)	87.4	92.4	92.4
residues in additionally allowed region (%)	10.9	7.6	7.6
residues in generously allowed region (%)	1.7	0.0	0.0

[a] Values in parentheses correspond to the highest resolution bin. [b] $R_{merge} = \sum|I_h - \langle I\rangle_h|/\sum I_h$, where $\langle I\rangle_h$ is average intensity over symmetry equivalents and h is the reflection index. [c] $R_{work} = \sum|F_c - F_o|/\sum F_o$.

respectively. Structural alignments with DALI (*31*) demonstrate that the TL1A monomer is most similar to the TNF family members CD40L (PDB code 1ALY) and TRAIL (PDB code 1D4V) with rmsds of 1.7 Å (136 C_αs) and 1.4 Å (135 C_αs), respectively. The β-sheet cores of these molecules superimpose well (Figure 2, Suporting Information Figure 2), with the greatest structural differences residing in the AA′, CD, and EF loop segments. The AA′ and CD loops of TL1A are significantly longer than those present in most TNF ligands, whereas its EF loop is shorter (Figure 1, Suporting Information Figure 2). Electron density for most of the CD loop (residues M91−N107) and the tip region of the AA′ (residues T40−Q46) loop is weak or absent, and as a result, these residues are not included in the final model of wild-type TL1A.

The asymmetric unit of the TL1A crystals contains a single protomer, which is orientated relative to the crystallographic 3-fold rotation axis to produce a tightly packed trimeric assembly that is typical of the TNF superfamily (Figure 2A). The solvent-accessible surface area of each protomer buried in the trimeric assembly is 1977 Å^2, comparable to that observed in other stable trimeric TNF ligands (TNFα, 2412 Å^2; TRAIL, 2261 Å^2; CD40L, 2091 Å^2). Similar to other conventional TNF ligands, the subunit interface of TL1A is formed by interactions between the edges of the β-sandwich in one protomer (E and F strands) and the inner sheet of the neighboring protomer (A, H, C, and F strands). The central region of this interface is composed predominantly of hydrophobic residues (Figure 3), with F81, Y146, F182, and L184 from each protomer positioned to contribute to the hydrophobic core of the trimer. The corresponding residues at these four positions in other conventional TNF ligands are generally conserved and form the most prevalent interdomain hydrophobic contacts (*32*). In addition, M150 from one protomer (F strand) and L58 and F142 from the adjacent protomer (AA′ loop and the F strand) contribute to the interface. The bottom of the TL1A subunit interface is lined with polar residues and is stabilized by six salt bridges and three hydrogen bonds. As a consequence of the short EF loop, the top of the TL1A trimer has relatively few intersubunit interactions compared to the significant number of predominantly polar interactions present in this region in TNFα (*32*). The structure of Jin et al. (*28*) showed three backbone hydrogen bonds at the top of TL1A subunit interface, which are absent in our structure due to disorder in the CD loop.

Solution Behavior. Size exclusion chromatography of TL1A yielded an apparent molecular mass of approximately 66 kDa (Figure 4A). With the exception of the E53A-E55A mutant, all mutants examined, including the R99A-R103A-D108A triple mutant and the Y121F single mutant, exhibited size exclusion chromatographic behavior similar to that of the native trimer, strongly indicating that these constructs exist as stable trimers in solution with interprotomer interactions similar to those of the wild type (Suporting Information Figure 5C). The observation of trimeric species is strong evidence that these mutant proteins adopt correct tertiary and quaternary structures and are thus capable of interacting with DcR3 in a productive manner. In contrast, E53A-E55A exhibits a monomer−oligomer equilibrium, suggesting these residues may be important for maintaining the oligomeric state (Suporting Information Figure 5D).

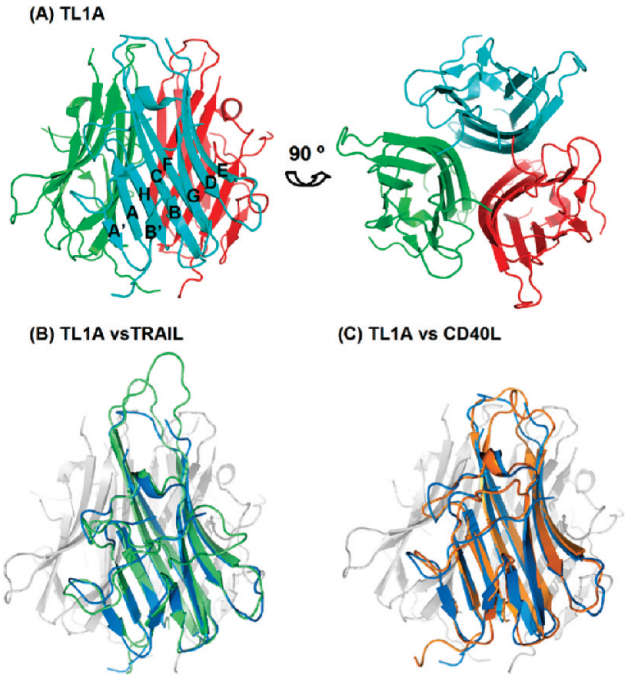

FIGURE 2: Ribbon structure of TL1A trimer assembly. (A) The three chains of TL1A are individually colored in cyan, green, and red. The right panel is rotated by 90° around the horizontal axis relative to the left panel. The β-stands are labeled as shown in Figure 1. Each loop is referenced in the text by the two strands connected to that loop. (B, C) Superimpositions of the TL1A structure with TRAIL and CD40L. TL1A is colored in blue and gray, TRAIL is in green, and CD40L is in orange.

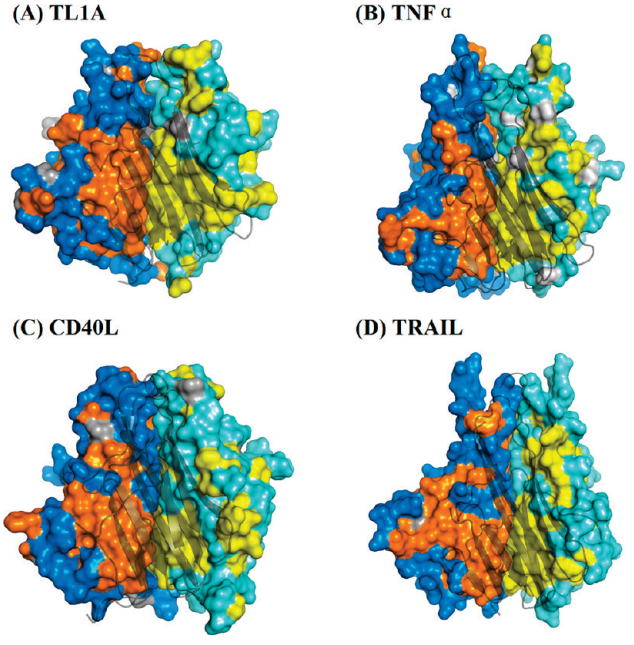

FIGURE 3: Different quaternary structures of TNF family members. Two protomers of each trimer assembly (TL1A, TNFα, PDB code 2TNF; CD40L, PDB code 1ALY; and TRAIL, PDB code 1D4V) are shown as surface representation, and the third protomer above is shown as a transparent ribbon. Hydrophobic/hydrophilic residues are colored in orange/blue in one protomer and yellow/cyan in the neighboring protomer.

Velocity sedimentation experiments with the wild-type TL1A yielded an $s°_{20,w}$ of 4.227 ± 0.013 S (Figure 4B), which corresponds to an apparent molecular mass (S/D) of 63.05 ± 1.63 kDa. These values are consistent with the calculated molecular mass of

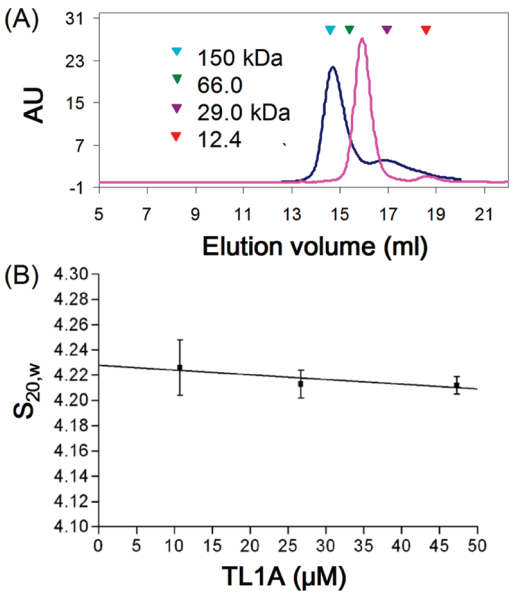

FIGURE 4: (A) Gel filtration of TL1A and the DcR3/TL1A(C95S/C135S) complex. The chromatogram for TL1A alone is drawn in purple and that for the DcR3/TL1A(C95S/C135S) mixture in blue. The elution profile of the wild-type TL1A/DcR3 mixture is similar to that of TL1A(C95S/C135S)/DcR3 (data not shown). The calculated molecular masses of the TL1A trimer and the DcR3 cysteine-rich domain are 62.67 and 20.1 kDa, respectively. The cyan, green, purple, and red arrowheads indicate the positions of standards with molecular masses of 150, 66, 29, and 12.4 kDa, respectively. (B) Velocity sedimentation analysis of TL1A. Sedimentation coefficients of TL1A were measured at three concentrations of the protein: 10.7, 26.7, and 47.3 μM.

the purified TL1A trimer (62.67 kDa). Increasing the TL1A concentration (10.7 μM to 47.3 μM) results in a slight decrease of $s_{20,w}$ (Figure 4B), indicating that there is no significant self-association of the TL1A trimer at the concentrations examined. Sedimentation experiments with the TL1A cysteine mutants (i.e., C95S, C135S, C95S/C135S) at a concentration of 26.7 μM yielded $s_{20,w}$ values indistinguishable from that of the wild-type protein (data not shown), confirming that the cysteine connectivity does not contribute to the formation or maintenance of the oligomeric state.

Solubility of TL1A. Long-term storage of recombinant TL1A requires reducing agents (for instance, 1 mm DTT) to prevent aggregation. Nonreducing SDS−PAGE analysis of the wild-type TL1A protein reveals three distinct species: a band corresponding to a dimer (~42 kDa) and two distinct lower molecular mass bands around the predicted monomer position (~21 kDa) (Figure 5 A, lane A). All three bands coalesce to a single monomeric species on reducing SDS−PAGE (data not shown), suggesting that the heterogeneity observed in nonreducing conditions is the result of interchain and intrachain disulfide bonds. Mutation of either or both of the cysteines in TL1A (i.e., C95S, C135S, and C95S/C135S) results in proteins resistant to aggregation in the absence of reducing agents. Nonreducing SDS−PAGE gel shows that the C135S protein is completely homogeneous (Figure 5A, lane C). However, the C95S mutant still possesses a dimer population (Figure 5A, lane B). These observations suggest that the lower monomer band associated with the wild-type protein might result from an intrachain disulfide bond between the CD and EF loops (Figure 5C) as observed in the structure of Jin et al. (*28*), while the dimer band might be the consequence of a disulfide bond formed by two

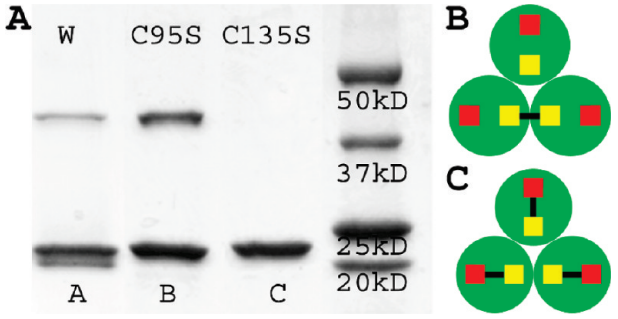

FIGURE 5: Disulfide bond content. (A) Nonreducing SDS−PAGE for wild-type TL1A native protein (lane A) and C95S (lane B) and C135S (lane C) mutants. The protein standard ladder is shown on the right side. (B, C) Models of disulfide connectivity. Each TL1A subunit is represented by a green circle; C95 and C135 are represented by red and yellow squares, respectively. Putative disulfide bonds are shown as black sticks.

C135 residues located in the EF loops of adjacent protomers in the homotrimer assembly (Figure 5B). The simultaneous presence of monomer and covalently linked dimer populations in native C95S mutant protein (demonstrated in Figure 5A, lane B) was confirmed by thermo Electron LTQ mass spectroscopy (data not shown). Nonreducing SDS−PAGE analysis of the C95S mutant TL1A crystals shows the same pattern observed in solution (data not shown), demonstrating that a particular species did not preferentially crystallize and that the crystals contain disulfide-linked protomers as well as reduced protomers.

Nonreducing SDS−PAGE gels of the wild-type TL1A protein indicate that the dimer population is about 20% of the total protein (Figure 5). In the structure of wild-type TL1A, C135 from the three protomers of the same homotrimer are in close proximity, with a distance of about 3.9 Å between adjacent sulfur atoms (7.6 Å between C_αs). Due to this mixture of disulfide-linked and reduced protomers, as well as inherent dynamics, the electron density of the EF loop containing C135 is weak and is compatible with the presence of a 20% population of linked protomers, which would be below the level of detection.

The C95S and C95S/C135S mutant proteins crystallized under similar conditions as the wild-type protein and are isomorphous with the wild-type crystals (Table 1). However, the mutant protein crystals are significantly larger in size and exhibited higher quality diffraction (Table 1). All three structures are similar with rmsd between coordinates of their C_α atoms about 0.6 Å (Suporting Information Figure 4). The biggest differences reside in the structurally dynamic EF loops. In all structures, the CD loops and the tip segment of the AA′ loops were disordered. Sedimentation velocity measurements demonstrate that all cysteine mutants (C95S, C135S, and C95S/C135S) are tight nondissociating trimers in solution (data not shown). The TL1A structure reported by Jin et al. shows the C95S−C135S disulfide bond with the complete CD loop being present in the model (*28*). Therefore, the disulfide bond heterogeneity in our crystals may lead to disorder in the CD loop and to flexibility of the EF loops. However, sedimentation velocity experiments show that this disulfide bond heterogeneity does not alter the quaternary structure of TL1A.

Interaction of Soluble hTL1A with hDcR3. The interactions of wild-type human TL1A with the human neutralizing receptor hDcR3 were evaluated using surface plasmon resonance (SPR) (Suporting Information Figure 3). The analysis of interaction between hDcR3 and wild-type TL1A yielded an equilibrium dissociation constant (K_d) of 1.1 nM, which is consistent with the previously reported value of 1.8 nM (*1*). In gel filtration studies, a 1:1 mixture of DcR3 cysteine-rich domain (CRD) and TL1A C95S/C135S double mutant results in a single species with significantly higher apparent molecular mass compared to TL1A alone (Figure 4A), reflecting tight binding between the two proteins and putative 3:3 binding stoichiometry. SPR analyses for the three TL1A cysteine mutants (C95S and C135S single mutants and C95S/C135S double mutant) resulted in binding affinities comparable to those of the wild-type TL1A, with K_ds ranging from 0.6 to 1.8 nM (Suporting Information Figure 3). These findings indicate that the absence of the C95−C135 disulfide link and the possible presence of interprotomer disulfide bonds do not effect the interaction between human TL1A and DcR3.

Thermal Stability. To map the DcR3-binding sites on TL1A, a series of residues on the surface of the TL1A C95S/C135S mutant were altered on the basis of sequence conservation and structural position. The stability of these mutants was examined by thermal melting experiment. All of the mutants, except G57D and E53A-E55A, exhibited melting temperatures that were equivalent to or higher than that exhibited by the C95S-C135S mutant (T_m = 77°). The G57D single mutant and E53A-E55A double mutant, both of which are located at the C-terminal base of the AA′ loop near the interprotomer interface, exhibited significantly lower melting temperatures (T_m = 47−49°). (Suporting Information Figure 5E,F).

DcR3-Binding Surface on TL1A. The ability of TL1A mutants to bind DcR3 was evaluated by SPR at a ligand concentration of 10 nM. As shown in Figure 6, the E53A-E55A double mutant and the G57D single mutant in the C-terminal base of the AA′ loop, the Y121F mutant in the DE loop, and the E174A single and K173A-K176A double mutants in the GH loop all showed significantly impaired interactions with the DcR3 decoy receptor. Several other mutants, including the L56A mutant in the AA′ loop, the S119A-E123A double mutant in the DE loop, and the K173A and D175A single mutants in the GH loop showed very modest decreases in DcR3 binding.

SPR kinetic analysis of the interaction between DcR3 and the R99A-R103A-D108A triple mutant in the CD loop yielded a K_d of 0.52 nM, essentially indistinguishable from that of the C95S-C135S TL1A mutant (K_d of 0.66 nM) (Suporting Information Figure 5). By contrast, the K_d of the Y121F single mutant is 6.75 nM, about 10-fold increase (Suporting Information Figure 5), and is consistent with the results depicted in Figure 6. These quantitative results serve to validate the use of maximal Biacore responses to provide qualitative data that are mechanistically informative.

The thermal dentauration studies suggest that the mutations at the C-terminal base of the AA′ loop (E53-E55 and G57) may indirectly influence DcR3 binding through effects in protein stability and/or oligomeric state. By contrast, the Y121F, E174A, and K173A-K176 mutants in the DE loop and GH loop have equivalent or even higher melting temperatures compared with the wild-type protein, suggesting that these residues are directly involved in DcR3 binding. Overall, these results indicate that the DE loop and GH loop of TL1A are involved in the binding of DcR3 receptor and the C-termial base of the AA′ loop is important for structural stability and oligomeric state of the protein.

DISCUSSION

Structure and Conservation. The current work demonstrates that the TL1A ectodomain adopts a typical TNF family

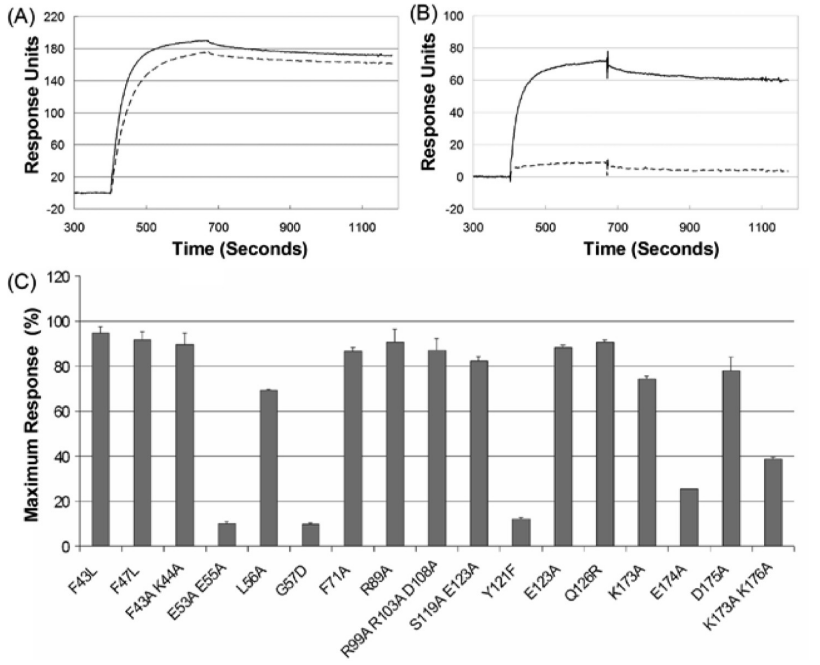

FIGURE 6: DcR3 binding determinants. A series of residues on the surface of the TL1A C95S/C135S double mutant were mutated, and their binding to the DcR3 receptor was assessed by SPR. (A) The sensorgram of the R99A-R103A-D108A triple mutant: solid line, wild type; dashed line, R99A-R103A-D108A triple mutant. (B) The sensorgram of the Y121F single mutant: solid line, wild type; dashed line, Y121F single mutant. (C) The effects of all mutations on DcR3 binding affinity relative to the wild type. The maximum association response of each mutant is divided by that of the wild-type TL1A and represented in the histogram as percentage of wild-type binding response. Vertical bars on each column represent the standard errors between two replicated measurements.

"jelly-roll" fold and exists as a stable trimer in both the solution and the crystalline state. As depicted in Figures 2 and 3, the TL1A interprotomer interface is formed by two layers of hydrophobic and hydrophilic interactions located at the middle and the bottom of the molecule, respectively. The top of the TL1A trimer is mainly composed of hydrophilic residues, but there are fewer interprotomer contacts in this region. This organization contrasts other conventional TNF family members which utilize three layers of alternating hydrophilic, hydrophobic, and hydrophilic interactions (represented by TNFα, CD40L, and TRAIL in Figure 3). More generally, the physicochemical properties of the interprotomer interfaces are distinct in each TNF family member, providing a mechanism that prevents inappropriate heterotrimer formation and enforces homotrimer formation.

The current structure allows for the generation of a structure-based sequence alignment, which highlights a number of residues that are invariant among the conventional TNF ligands (shown as red positions in Figure 1). W52, L72, Y80, L153, and F179 (TL1A numbering) are invariant, likely due to their contribution to the hydrophobic core of each protomer (Suporting Information Figure 6). The invariant G78 residue is located at the base of the BC loop and adopts a dihedral angle that is unfavorable for other amino acids but is required to support the connection between the BC loop and C strand (Suporting Information Figure 6). Y83, G148, and G180 are also invariant due to their contributions to the interprotomer interface. *In silico* mutation of G148 to alanine results in a steric clash with the side chain of F81 from the same protomer, which is part of the hydrophobic core at the trimer interface. The side chain of Y83 extends toward the neighboring β-sheet, occupying the available space above G180, and its phenolic hydroxyl group forms hydrogen bonds with the side chain of the nearly invariant H31 from the same protomer and the backbone amide of M150 from the adjacent protomer (Suporting Information Figure 7). These inter/intraprotomer interactions involving Y83 are conserved among all of the conventional TNF ligands with known structures (TNFα, LTα, TRAIL, and CD40L).

Disulfide Bonds. The two cysteines present in the CD and EF loops of TL1A are conserved among most conventional TNF ligands (Figure 1). Because TNFα and CD40L both possess intramolecular disulfide bonds connecting these two loops (*32*), LIGHT, FasL, and TL1A were all predicted to have similar disulfide connectivity (*33*). As described above, recombinant wild-type TL1A protein produced in *E. coli* appears to be heterogeneous in terms of disulfide bond content, with both an intrachain disulfide bond between the CD loop and EF loop and an interchain disulfide bond between the EF loops from adjacent protomers in the same homotrimer assembly. Sedimentation velocity measurements of the cysteine mutants reveal that they all have the same quaternary structure as the wild-type protein. Based on the nearly identical binding of wild-type and the C95S/C135S mutant TL1A to DcR3 (Figure 4A, Suporting Information Figure 3), these cysteines and the associated disulfide linkages are not critical for structural integrity or DcR3 binding. Interestingly, a small fraction of naturally secreted human TL1A also has interchain disulfide bonds (*34*), reflecting the *in vivo* occurrence of TL1A disulfide bond heterogeneity. However, since the intrachain disulfide bond between the CD loop and EF loop is present in the TL1A structure reported by Jin et al. (*28*), the disulfide bond heterogeneity observed in our structure may in part be the consequence of our recombinant expression protocol in *E. coli*. Importantly, since all three TL1A cysteine mutants described above are more resistant to aggregation than the wild-type protein expressed in *E. coli*, they provide superior and more economical alternatives for future mechanistic and clinical studies.

DcR3 Binding Interface. The existing structures of TNF:TNFR family complexes suggest a common mechanism for

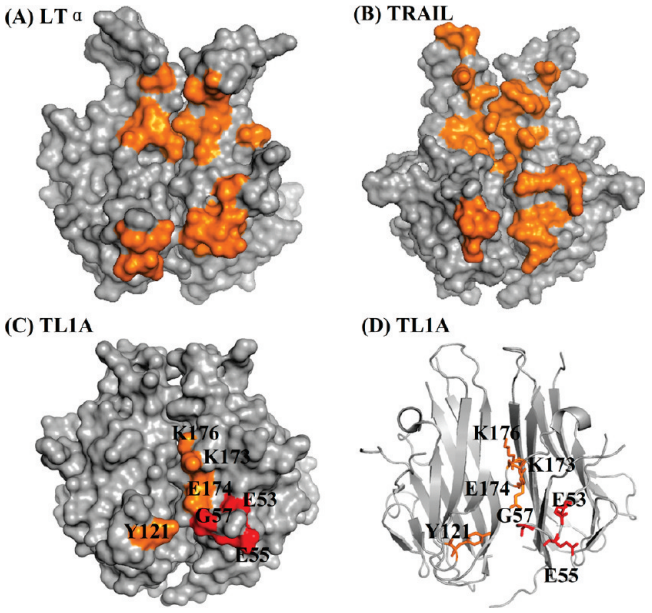

FIGURE 7: Receptor binding interfaces in TNF ligands. In the upper two panels, orange patches indicate the surfaces of LTα (panel A, PDB code 1TNR) and TRAIL (panel B, PDB code 1D4V) that are involved in receptor binding based on cocrystal structures with their respective receptors (*17*). In the lower two panels, the residues important for the TL1A−DcR3 interaction, based on mutagenesis studies, are shown in orange as a surface representation in panel C and stick representation in panel D. The residues that may indirectly impact interaction with DcR3 through effects on protein stability or oligomeric state are shown in red.

receptor recognition and provide considerable insights into the receptor binding surfaces on the ligands. In particular, the receptors interact with solvent-accessible segments that form the groove between two adjacent ligand protomers. In TRAIL and LTα, as depicted in panels A and B of Figure 7, the receptor binding surfaces can be divided into two regions: the lower level composed of the DE and AA′ loops and the upper level mainly formed by the CD loop (Figure 7) (*17*, *35*). This conservation in the receptor binding interface allows for the prediction of the TL1A surfaces involved in the recognition of the functional DR3 receptor and the neutralizing DcR3 receptor.

In the lower region of the receptor binding groove of TL1A, Y121 located at the tip of the DE loop (Figure 7C,D) is one of the most conserved residues among conventional TNF ligands (Figure 1). Structural alignments reveal that these conserved tyrosines are located very close in space with similar conformations (Suporting Information Figure 8). In the structures of the LTα/TNFR1 and TRAIL/DR5 complexes, the phenolic hydroxyl groups from these conserved tyrosines participate in hydrogen-bonding interactions with the backbone atoms of their cognate receptors (*16*, *17*), and mutagenesis studies demonstrate that alteration of this tyrosine residue in TNFα, LTα, FasL, LIGHT, and TRAIL results in dramatic decreases in receptor binding affinity (*36*−*40*). Consistent with a conserved role of this tyrosine in TNF family function, Y121 in TL1A is situated at the bottom of the putative binding groove (Figure 7) with considerable solvent-accessible surface area (141 $Å^2$), and the Y121F mutation reduces TL1A binding to DcR3 by 90% (Figure 6). Interestingly, two other conventional TNF ligands, RANKL and CD40L, possess Ile and Arg instead of Tyr in this position, respectively (Figure 1), suggesting some variability in the detailed mechanisms of receptor recognition.

In contrast to the significant impact of Y121F mutation in TL1A, the substitutions of other conserved residues in the DE loop (E123A single mutant and S120A-E123A double mutant) do not significantly affect TL1A binding to DcR3 (Figure 6). In the structure of the TRAIL/DR5 complex, S215 and D218 of TRAIL (counterparts of TL1A S120 and E123, respectively) both form polar interactions with side chains of H106 and D109 on the DR5 receptor (*17*). However, the analogous region of DcR3 (residues F80−Y83) is composed mainly of hydrophobic residues (Suporting Information Figure 9), precluding polar interactions with the side chains of S120 and E123. It is thus likely that Y121 is the predominant contributor of the TL1A DE loop to DcR3 binding. Notably, the analogous segment in DR3 contains several hydrophilic residues (E82, H84, and H85) that can potentially participate in polar interactions with the side chains of S120 and E123 in TL1A, suggesting detailed differences in the mechanisms used to recognize the two receptors.

The C-terminal end of the AA′ loop in conventional TNF ligands is positioned at the same relative height within the trimer as the DE loop (Figure 7 and Suporting Information Figure 2) and represents another critical region in the lower level of the receptor binding interface (*40*). Residues corresponding to TL1A residues E53 and G57 are among the most conserved in the receptor binding groove of the TNF family ligands. In TL1A, the E53A-E55A double mutant and the G57D single mutant both exhibited substantial losses of binding affinity for DcR3 (Figure 6). Similarly, mutation of the G57 analogue in LTα (D50) dramatically decreased the affinity of receptor binding (*38*). The equivalent of TL1A E53 in TRAIL is E155, and its side chain forms a salt bridge with the R115 guanidine group of the DR5 receptor (*17*). This Arg is conserved in DR3 but is substituted by Tyr in DcR3 (Y89 in Suporting Information Figure 9). Thus, compared with the TRAIL/DR5 structure, E53-E55 in TL1A might interact with DcR3 in a different fashion. Notably, the gel filtration and thermal melting experiments suggest that G57D and E53A-E55A mutants may contribute to DcR3 binding through destabilizing the protein structure or altering the oligomeric state (Suporting Information Figure 5D,E,F).

In addition to the C-terminal end of the AA′ loop, the TRAIL/DR5 structure shows that the middle region of the extended TRAIL AA′ loop also plays an important role in receptor binding (*17*). This interaction is precluded in the LTα/TNFR1 structure because of a shorter AA′ loop (*17*). Similar to TRAIL, TL1A also possesses a relatively long AA′ loop (Figure 1). However, mutations in the middle region of this loop (i.e., F43A-K44A double mutant) did not change the DcR3 binding affinity, suggesting that the C-terminal end of the AA′ loop in TL1A provides the most important binding determinants in this loop.

The upper level of the receptor binding interfaces in both TRAIL and LTα is formed predominately by contributions from the CD loops (Figure 7). Compared with most TNF ligands, the CD loop in TL1A is significantly longer (Figure 1, Suporting Information Figure 2). The R89A single mutation and R99A-R103A-D108A triple mutation in the TL1A CD loop have no effect on the interaction between TL1A and DcR3 (Figure 6). These results again indicate differences in receptor recognition between TL1A and TRAIL/LTα and suggest that the CD loop of TL1A may not serve as part of the receptor binding interface. Importantly, due to the limitations of mutagenesis approaches, at this point, we cannot exclude interactions contributed by the backbone atoms of TL1A to the binding interface.

In the "center" of the receptor binding groove of TL1A, K173, E174, D175, and K176 contributed from the tip of the GH loop form a region with considerable ionic character (Figure 7). In most TNF ligands this region is composed of charged or hydrophilic residues (Figure 1); however, neither LTα nor TRAIL utilize this region for receptor binding(*16*, *17*). In TL1A, the E174A single mutant and K173A-K176A double mutant both significantly reduced the DcR3 binding affinity (Figure 6), suggesting additional differences in TL1A−DcR3 recognition compared to other family members.

The structural and mutagenesis studies map the DcR3-binding surface of TL1A and show both common and unique features compared with known TNF ligand−receptor complexes. The DcR3-binding interface appears to involve the surface of the lower half of the groove formed between two TL1A protomers, with additional contributions from the central region but few interactions involving the upper half of the TL1A molecule (Figure 7C). These features suggest an asymmetric interaction pattern for DcR3 along the interprotomer groove in TL1A. By contrast, other TNF ligands interact with their cognate receptors in more symmetrical fashion, such that the bound receptor runs parallel to the ligand 3-fold symmetry axis with the interaction surfaces evenly distributed along the lower and upper parts of the ligand. Notably, potential interactions between the side chain atoms of the TL1A DE loop and DR3 suggest possible differences in TL1A recognition by the functional receptor DR3 and decoy receptor DcR3. Finally, and most intriguingly, the apparent asymmetric interaction between DcR3 and TL1A may be an important element for the unique ability of DcR3 to recognize and neutralize multiple TNF ligands (i.e., TL1A, LIGHT, and FasL).

In summary, our structural and biochemical data confirm the stable trimeric assembly of the TL1A cytokine, map the DcR3 binding sites on TL1A, predict interactions that might contribute to binding specificity, and highlight unique features of the TL1A−DcR3 interaction that may be important for biological function. We also characterized a series of TL1A cysteine mutants with enhanced solution properties that are structurally and functionally similar to those of the wild-type protein. Together, these findings provide important tools and insights for the further mechanistic dissection of TNF/TNFR function.

ACKNOWLEDGMENT

We gratefully acknowledge the staff of the X29 beamline at the National Synchrotron Light Source for assistance in data collection and Dr. Hui Xiao at the Laboratory for Macromolecular Analysis and Proteomics, Albert Einstein College of Medicine, for assistance with mass spectroscopy.

SUPPORTING INFORMATION AVAILABLE

Protocols for DcR3 expression and purification and structural comparison, illustrations for structural superimposition of TL1A with conventional TNF ligands, highly conserved residues in TL1A and TNF receptor sequence alignment, kinetic analysis of the interaction between immobilized DcR3−Ig fusion protein and TL1A mutants, and thermal stability of TL1A mutants. This material is available free of charge via the Internet at http://pubs.acs.org.

REFERENCES

1. Migone, T. S., Zhang, J., Luo, X., Zhuang, L., Chen, C., Hu, B., Hong, J. S., Perry, J. W., Chen, S. F., Zhou, J. X., Cho, Y. H., Ullrich, S., Kanakaraj, P., Carrell, J., Boyd, E., Olsen, H. S., Hu, G., Pukac, L., Liu, D., Ni, J., Kim, S., Gentz, R., Feng, P., Moore, P. A., Ruben, S. M., and Wei, P. (2002) TL1A is a TNF-like ligand for DR3 and TR6/DcR3 and functions as a T cell costimulator. *Immunity 16*, 479–492.
2. Chew, L. J., Pan, H., Yu, J., Tian, S., Huang, W. Q., Zhang, J. Y., Pang, S., and Li, L. Y. (2002) A novel secreted splice variant of vascular endothelial cell growth inhibitor. *FASEB J. 16*, 742–744.
3. Yang, C. R., Hsieh, S. L., Teng, C. M., Ho, F. M., Su, W. L., and Lin, W. W. (2004) Soluble decoy receptor 3 induces angiogenesis by neutralization of TL1A, a cytokine belonging to tumor necrosis factor superfamily and exhibiting angiostatic action. *Cancer Res. 64*, 1122–1129.
4. Bamias, G., Mishina, M., Nyce, M., Ross, W. G., Kollias, G., Rivera-Nieves, J., Pizarro, T. T., and Cominelli, F. (2006) Role of TL1A and its receptor DR3 in two models of chronic murine ileitis. *Proc. Natl. Acad. Sci. U.S.A. 103*, 8441–8446.
5. Pappu, B. P., Borodovsky, A., Zheng, T. S., Yang, X., Wu, P., Dong, X., Weng, S., Browning, B., Scott, M. L., Ma, L., Su, L., Tian, Q., Schneider, P., Flavell, R. A., Dong, C., and Burkly, L. C. (2008) TL1A-DR3 interaction regulates Th17 cell function and Th17-mediated autoimmune disease. *J. Exp. Med. 205*, 1049–1062.
6. Meylan, F., Davidson, T. S., Kahle, E., Kinder, M., Acharya, K., Jankovic, D., Bundoc, V., Hodges, M., Shevach, E. M., Keane-Myers, A., Wang, E. C., and Siegel, R. M. (2008) The TNF-family receptor DR3 is essential for diverse T cell-mediated inflammatory diseases. *Immunity 29*, 79–89.
7. Bai, C., Connolly, B., Metzker, M. L., Hilliard, C. A., Liu, X., Sandig, V., Soderman, A., Galloway, S. M., Liu, Q., Austin, C. P., and Caskey, C. T. (2000) Overexpression of M68/DcR3 in human gastrointestinal tract tumors independent of gene amplification and its location in a four-gene cluster. *Proc. Natl. Acad. Sci. U.S.A. 97*, 1230–1235.
8. Pitti, R. M., Marsters, S. A., Lawrence, D. A., Roy, M., Kischkel, F. C., Dowd, P., Huang, A., Donahue, C. J., Sherwood, S. W., Baldwin, D. T., Godowski, P. J., Wood, W. I., Gurney, A. L., Hillan, K. J., Cohen, R. L., Goddard, A. D., Botstein, D., and Ashkenazi, A. (1998) Genomic amplification of a decoy receptor for Fas ligand in lung and colon cancer. *Nature 396*, 699–703.
9. Yu, K. Y., Kwon, B., Ni, J., Zhai, Y., Ebner, R., and Kwon, B. S. (1999) A newly identified member of tumor necrosis factor receptor superfamily (TR6) suppresses LIGHT-mediated apoptosis. *J. Biol. Chem. 274*, 13733–13736.
10. Hsu, T. L., Wu, Y. Y., Chang, Y. C., Yang, C. Y., Lai, M. Z., Su, W. B., and Hsieh, S. L. (2005) Attenuation of Th1 response in decoy receptor 3 transgenic mice. *J. Immunol. 175*, 5135–5145.
11. Wu, S. F., Liu, T. M., Lin, Y. C., Sytwu, H. K., Juan, H. F., Chen, S. T., Shen, K. L., Hsi, S. C., and Hsieh, S. L. (2004) Immunomodulatory effect of decoy receptor 3 on the differentiation and function of bone marrow-derived dendritic cells in nonobese diabetic mice: from regulatory mechanism to clinical implication. *J. Leukocyte Biol. 75*, 293–306.
12. Hsu, T. L., Chang, Y. C., Chen, S. J., Liu, Y. J., Chiu, A. W., Chio, C. C., Chen, L., and Hsieh, S. L. (2002) Modulation of dendritic cell differentiation and maturation by decoy receptor 3. *J. Immunol. 168*, 4846–4853.
13. Takahama, Y., Yamada, Y., Emoto, K., Fujimoto, H., Takayama, T., Ueno, M., Uchida, H., Hirao, S., Mizuno, T., and Nakajima, Y. (2002) The prognostic significance of overexpression of the decoy receptor for Fas ligand (DcR3) in patients with gastric carcinomas. *Gastric Cancer 5*, 61–68.
14. Sung, H. H., Juang, J. H., Lin, Y. C., Kuo, C. H., Hung, J. T., Chen, A., Chang, D. M., Chang, S. Y., Hsieh, S. L., and Sytwu, H. K. (2004) Transgenic expression of decoy receptor 3 protects islets from spontaneous and chemical-induced autoimmune destruction in nonobese diabetic mice. *J. Exp. Med. 199*, 1143–1151.
15. Compaan, D. M., and Hymowitz, S. G. (2006) The crystal structure of the costimulatory OX40-OX40L complex. *Structure 14*, 1321–1330.
16. Banner, D. W., D'Arcy, A., Janes, W., Gentz, R., Schoenfeld, H. J., Broger, C., Loetscher, H., and Lesslauer, W. (1993) Crystal structure of the soluble human 55 kd TNF receptor-human TNF beta complex: implications for TNF receptor activation. *Cell 73*, 431–445.
17. Mongkolsapaya, J., Grimes, J. M., Chen, N., Xu, X. N., Stuart, D. I., Jones, E. Y., and Screaton, G. R. (1999) Structure of the TRAIL-DR5 complex reveals mechanisms conferring specificity in apoptotic initiation. *Nat. Struct. Biol. 6*, 1048–1053.
18. Hymowitz, S. G., Christinger, H. W., Fuh, G., Ultsch, M., O'Connell, M., Kelley, R. F., Ashkenazi, A., and de Vos, A. M. (1999) Triggering cell death: the crystal structure of Apo2L/TRAIL in a complex with death receptor 5. *Mol. Cell 4*, 563–571.

19. Locksley, R. M., Killeen, N., and Lenardo, M. J. (2001) The TNF and TNF receptor superfamilies: integrating mammalian biology. *Cell 104*, 487–501.
20. Kang, Y. J., Kim, W. J., Bae, H. U., Kim, D. I., Park, Y. B., Park, J. E., Kwon, B. S., and Lee, W. H. (2005) Involvement of TL1A and DR3 in induction of pro-inflammatory cytokines and matrix metalloproteinase-9 in atherogenesis. *Cytokine 29*, 229–235.
21. Borysenko, C. W., Furey, W. F., and Blair, H. C. (2005) Comparative modeling of TNFRSF25 (DR3) predicts receptor destabilization by a mutation linked to rheumatoid arthritis. *Biochem. Biophys. Res. Commun. 328*, 794–799.
22. Yamazaki, K., McGovern, D., Ragoussis, J., Paolucci, M., Butler, H., Jewell, D., Cardon, L., Takazoe, M., Tanaka, T., Ichimori, T., Saito, S., Sekine, A., Iida, A., Takahashi, A., Tsunoda, T., Lathrop, M., and Nakamura, Y. (2005) Single nucleotide polymorphisms in TNFSF15 confer susceptibility to Crohn's disease. *Hum. Mol. Genet. 14*, 3499–3506.
23. Young, H. A., and Tovey, M. G. (2006) TL1A: a mediator of gut inflammation. *Proc. Natl. Acad. Sci. U.S.A. 103*, 8303–8304.
24. Otwinowski, Z., and Minor, W. (1997) Processing of X-ray diffraction data collected in oscillation mode. *Methods Enzymol. 276*, 307–326.
25. Storoni, L. C., McCoy, A. J., and Read, R. J. (2004) Likelihood-enhanced fast rotation functions. *Acta Crystallogr., Sect. D: Biol. Crystallogr. 60*, 432–438.
26. Evrard, G. X., Langer, G. G., Perrakis, A., and Lamzin, V. S. (2007) Assessment of automatic ligand building in ARP/wARP. *Acta Crystallogr., Sect. D: Biol. Crystallogr. 63*, 108–117.
27. Murshudov, G. N., Vagin, A. A., and Dodson, E. J. (1997) Refinement of macromolecular structures by the maximum-likelihood method. *Acta Crystallogr., Sect. D: Biol. Crystallogr. 53*, 240–255.
28. Jin, T., Guo, F., Kim, S., Howard, A., and Zhang, Y. Z. (2007) X-ray crystal structure of TNF ligand family member TL1A at 2.1 Å. *Biochem. Biophys. Res. Commun. 364*, 1–6.
29. Philo, J. S. (2000) A method for directly fitting the time derivative of sedimentation velocity data and an alternative algorithm for calculating sedimentation coefficient distribution functions. *Anal. Biochem. 279*, 151–163.
30. Laue, T. M., Shah, B. D., Ridgeway, T. M., Pelletier, S. L. (1991) Analytical Ultracentrifugation in Biochemistry and Polymer Science , Royal Society for Chemistry, Cambridge, U.K.
31. Holm, L., and Park, J. (2000) DaliLite workbench for protein structure comparison. *Bioinformatics 16*, 566–567.
32. Eck, M. J., and Sprang, S. R. (1989) The structure of tumor necrosis factor-alpha at 2.6 Å resolution. Implications for receptor binding. *J. Biol. Chem. 264*, 17595–17605.
33. Bodmer, J. L., Meier, P., Tschopp, J., and Schneider, P. (2000) Cysteine 230 is essential for the structure and activity of the cytotoxic ligand TRAIL. *J. Biol. Chem. 275*, 20632–20637.
34. Kim, S., and Zhang, L. (2005) Identification of naturally secreted soluble form of TL1A, a TNF-like cytokine. *J. Immunol. Methods 298*, 1–8.
35. Bodmer, J. L., Schneider, P., and Tschopp, J. (2002) The molecular architecture of the TNF superfamily. *Trends Biochem. Sci. 27*, 19–26.
36. Yamagishi, J., Kawashima, H., Matsuo, N., Ohue, M., Yamayoshi, M., Fukui, T., Kotani, H., Furuta, R., Nakano, K., and Yamada, M. (1990) Mutational analysis of structure−activity relationships in human tumor necrosis factor-alpha. *Protein Eng. 3*, 713–719.
37. Schneider, P., Bodmer, J. L., Holler, N., Mattmann, C., Scuderi, P., Terskikh, A., Peitsch, M. C., and Tschopp, J. (1997) Characterization of Fas (Apo-1, CD95)-Fas ligand interaction. *J. Biol. Chem. 272*, 18827–18833.
38. Goh, C. R., Loh, C. S., and Porter, A. G. (1991) Aspartic acid 50 and tyrosine 108 are essential for receptor binding and cytotoxic activity of tumour necrosis factor beta (lymphotoxin). *Protein Eng. 4*, 785–791.
39. Hymowitz, S. G., O'Connell, M. P., Ultsch, M. H., Hurst, A., Totpal, K., Ashkenazi, A., de Vos, A. M., and Kelley, R. F. (2000) A unique zinc-binding site revealed by a high-resolution X-ray structure of homotrimeric Apo2L/TRAIL. *Biochemistry 39*, 633–640.
40. Rooney, I. A., Butrovich, K. D., Glass, A. A., Borboroglu, S., Benedict, C. A., Whitbeck, J. C., Cohen, G. H., Eisenberg, R. J., and Ware, C. F. (2000) The lymphotoxin-beta receptor is necessary and sufficient for LIGHT-mediated apoptosis of tumor cells. *J. Biol. Chem. 275*, 14307–14315.